OPEN ACCESS
Journal of Innovative Optical Health Sciences
Vol. 16, No. 4 (2023) 2250040 (15 pages)

DOI: 10.1142/S1793545822500407

World Scientific
www.worldscientific.com

# Study on the secondary structure and hydration effect of human serum albumin under acidic pH and ethanol perturbation with IR/NIR spectroscopy

Hui Zhang[*,†,‖], Mengying Liang[*,‖], Shuangshuang Li[*], Mengyin Tian[*], Xiaoying Wei[*], Bing Zhao[*], Haowei Wang[*], Qin Dong[*,‡,¶] and Hengchang Zang[*,§,¶]

[*]*NMPA Key Laboratory for Technology Research and Evaluation of Drug Products*
*School of Pharmaceutical Sciences*
*Cheeloo College of Medicine, Shandong University*
*Wenhuaxi Road 44 Jinan, Shandong 250012, P. R. China*

[†]*National Glycoengineering Research Center*
*Shandong University, Jinan, Shandong 250012, P. R. China*
[‡]*qindong413@163.com*
[§]*zanghcw@126.com*

Received 24 October 2022
Revised 25 November 2022
Accepted 1 December 2022
Published 28 February 2023

Human serum albumin (HSA) is the most abundant protein in plasma and plays an essential physiological role in the human body. Ethanol precipitation is the most widely used way to obtain HSA, and pH and ethanol are crucial factors affecting the process. In this study, infrared (IR) spectroscopy and near-infrared (NIR) spectroscopy in combination with chemometrics were used to investigate the changes in the secondary structure and hydration of HSA at acidic pH (5.6–3.2) and isoelectric pH when ethanol concentration was varied from 0% to 40% as a perturbation. IR spectroscopy combined with the two-dimensional correlation spectroscopy (2DCOS) analysis for acid pH system proved that the secondary structure of HSA changed significantly when pH was around 4.5. What's more, the IR spectroscopy and 2DCOS analysis showed different secondary structure forms under different ethanol concentrations at the isoelectric pH. For the hydration effect analysis, NIR spectroscopy combined with the McCabe–Fisher method and aquaphotomics showed that the free hydrogen-bonded water fluctuates dynamically, with ethanol at 0–20% enhancing the hydrogen-bonded water clusters, while weak hydrogen-bonded water clusters were formed when the ethanol concentration increased continuously from 20% to 30%. These measurements provide new insights into the structural changes and changes in the hydration behavior of HSA, revealing the dynamic process of protein purification, and providing a

¶Corresponding authors.
‖Hui Zhang and Mengying Liang are co-first authors.

theoretical basis for the selection of HSA alcoholic precipitation process parameters, as well as for further studies of complex biological systems.

*Keywords*: Human serum albumin; hydration; formation; secondary structure; IR spectroscopy; NIR spectroscopy.

## 1. Introduction

As the most abundant protein in plasma, human serum albumin (HSA)[1] is synthesized and secreted by the liver and has physiological functions in transporting hormones, fatty acids, and various compounds.[2–4] Currently, the most widely large-scale preparation method for HSA is the cryogenic ethanol precipitation method created by Cohn in 1946.[5] The method is based on mixed plasma as raw material, decreasing the acidity step by step (from pH 7.0 to pH 4.0), increasing the ethanol concentration (from 0% to 40%), and decreasing the temperature (from 2°C to −2°C) to precipitate HSA from the solution step by step under different conditions. There is no doubt that pH and ethanol concentration are the key factors for the separation and purification of HSA in the ethanol precipitation process. Previous study[6] also proposed that the regulation of ethanol concentration and pH affect the hydrophobic interaction, electrostatic interaction, and hydrogen bond between proteins, which leads to the aggregation and precipitation of proteins. However, the mechanism of ethanol precipitation of HSA is not fully understood, which limits the access to high-quality HSA to some extent. The study of intermolecular interactions is one of the important fundamental works in the ethanol precipitation process of HSA, so a clearer understanding of the changes in intermolecular interactions of HSA caused by changes in pH and ethanol concentration, including changes in the secondary structure and hydration of proteins, is essential to obtain high-quality HSA.

Infrared (IR) spectroscopy (wavenumber in the range of 4000–500 $cm^{-1}$) is particularly sensitive to structural changes in proteins by revealing the IR spectral vibrations of peptide backbones or side chains.[7] Based on reflecting the absorption of the first overtone and combined frequency of C–H, O–H, and N–H, near-infrared (NIR) spectroscopy (wavenumber in the range of 12820–3959 $cm^{-1}$) has shown powerful functions in characterizing the structure and hydration of solution proteins.[8,9] Vanessa Moll *et al.* investigated the interaction of water with different hydrophobic polymers by NIR spectroscopy, revealing trends related to the chemistry of the polymers and their increasing hydrophilicity.[10] A simple NIR model was constructed by Chen Yu *et al.* to predict the concentration of ethanol in the actual production of immunoglobulin G online.[11] Mengli Fan *et al.* studied the structural changes of protein solutions using NIR spectroscopy.[12] and Li Ma *et al.* studied the function of water during protein gelation using NIR spectroscopy.[13] Therefore, IR spectroscopy and NIR spectroscopy are important molecular spectroscopic techniques that can be used to interpret the interaction between ethanol and HSA. It is worth mentioning that several chemometrics methods are necessary in spectroscopy analysis. Two-dimensional correlation spectroscopy (2DCOS) was first applied in the field of nuclear magnetic resonance (NMR),[14] and it has been widely used in protein research by increasing the spectral resolution and improving the determination of spectral intensity order changes.[15] Aquaphotomics, proposed by Professor Tsenkova of Kobe University in Japan in 2005,[16] is a study of using spectroscopic techniques to detect structural changes in water under different environments and to reflect the changes in other substances in the system at the molecular level and widely used in various aspects such as food,[17,18] pharmaceuticals,[19–21] medical,[22,23] industry,[24] testing industries,[25] and materials.[26,27]

The objective of this study was to obtain information on the state of the hydration layer surrounding HSA during ethanol precipitation in the acidic pH system and the isoelectric point, as well as the secondary structure of HSA. The three conformation structural forms of HSA in acidic pH system (pH 5.6–3.2) were studied with the 2DCOS and the moving window two-dimensional correlation spectroscopy (MW-2DCOS). The McCabe–Fisher method combined with aquaphotomics were utilized to analyze the hydration spectra of HSA and the molecular structure changes of HSA hydrated water. This study elucidated the mechanism of

ethanol precipitation of HSA at acidic and isoelectric point pH from the perspective of molecular spectroscopy, deepened the understanding of the structural change characteristics and hydration behavior changes in the alcoholic precipitation process of HSA, then provided a key scientific support for optimizing the production process and obtaining high-quality plasma protein products.

## 2. Materials and Methods

### 2.1. *Materials*

$H_3PO_4$ (about 99.9% purity), $NaH_2PO_4 \cdot 12\ H_2O$ (about 99.9% purity), Ethanol (about 99.9% purity), NaOH (about 99.9% purity), and $NaH_2PO_4 \cdot 2\ H_2O$ (about 99.9% purity) were acquired from Shanghai-Hushi (China). HSA (purity of more than 96% and Mw 66 kDa) was purchased from Sigma-Aldrich (Saint Louis, USA, #A9731).

### 2.2. *Sample preparation*

First, 0.2 mol/L $H_3PO_4$ solution and 0.2 mol/L $Na_2HPO_4$ solutions were prepared separately. Then, phosphate buffer solutions with pH 5.6–3.2 at intervals of 0.2 were prepared. The background solutions were prepared with 0.8 mL of each pH buffer and water was added to 1 mL each. The HSA solutions with pH 5.6–3.2 were obtained by adding 0.8 mL of each pH buffer and water to a concentration of 30 mg/mL.

Then, solution A (0.2 mol/L $NaH_2PO_4$ solution) and solution B (0.2 mol/L NaOH) were mixed into pH of 4.49 to obtain solution C. The HSA aqueous solution was adjusted to 60 mg/mL with solution C to obtain solution D. 37.5 mL of solution C was measured accurately, and 25 mL of water was added and mixed well to obtain HSA–buffer solutions. At last, the ethanol–buffer solutions were obtained by adding ethanol to the buffer at successive v/v levels (0–40% at 10% intervals, 30–33% at 3% intervals, and 35–38% at 3% intervals). HSA buffer solutions with pH of $4.60 \pm 0.05$ and different ethanol concentrations of 30 mg/mL were prepared, and then ethanol-HSA buffer solutions with the same v/v level were also prepared.

### 2.3. *Spectral measurement*

The IR spectra were acquired using an FT-IR spectrometer (Nicolet 6700, Thermo fisher scientific, USA) in the range of 4000–400 $cm^{-1}$ with a scan number of 64 and a resolution of 4 $cm^{-1}$ at 25°C. The signal-to-noise ratio was increased by collecting air spectra and subtracting them. Each sample was measured three times and averaged.

The NIR spectra were obtained using the Fourier-transform (FT) NIR spectrometer (Antaris II, USA) with a tungsten-halogen light source and an InGaAs detector in transmission mode from 10000–4000 $cm^{-1}$ using a 1 mm cuvette, a scan number of 64 and a resolution of 4 $cm^{-1}$ at 25°C. Each sample was measured three times and averaged.

### 2.4. *Data processing*

The data was processed with Matlab R2019a (The Math Works Inc., Natick, MA, USA).

## 3. Results and Discussion

### 3.1. *The pH-induced second structure of HSA*

#### 3.1.1. *The MIR and the difference spectra of HSA at pH 5.6–3.2*

To illustrate the effect of pH on the structure of HSA, the IR spectra of buffer solution and HSA buffer solution at different pH at 4000–500 $cm^{-1}$ are shown in Fig. 1(a). A significant broad absorption peak at 3200 $cm^{-1}$ could be observed in the spectrogram, which primarily attributed to the stretching vibrational absorption of O–H and N–H groups,[28,29] while a significant narrow absorption peak at 1640 $cm^{-1}$ was primarily associated with the absorption of bending vibration of the O–H group and stretching vibration of the C=O group of HSA.[30] In conventional IR spectral analysis, the spectral difference subtraction (difference spectrum) method is often used to reduce or even eliminate the interference of useless matrix substances and amplify the useful information. In this paper, in order to eliminate the interference caused by the strong absorption of the O–H group, the original spectrum was processed using the difference spectrum method. The HSA buffer solution spectrum minus the buffered solvent spectrum is shown in Fig. 1(b). The absorption peak located at 1652 $cm^{-1}$ mainly aroused by the vibrational absorption of the HSA amide I region[30] could be observed. 1750–1580 $cm^{-1}$ is close to the amide I band of the protein (1700–1600 $cm^{-1}$). While the amide I band is sensitive to

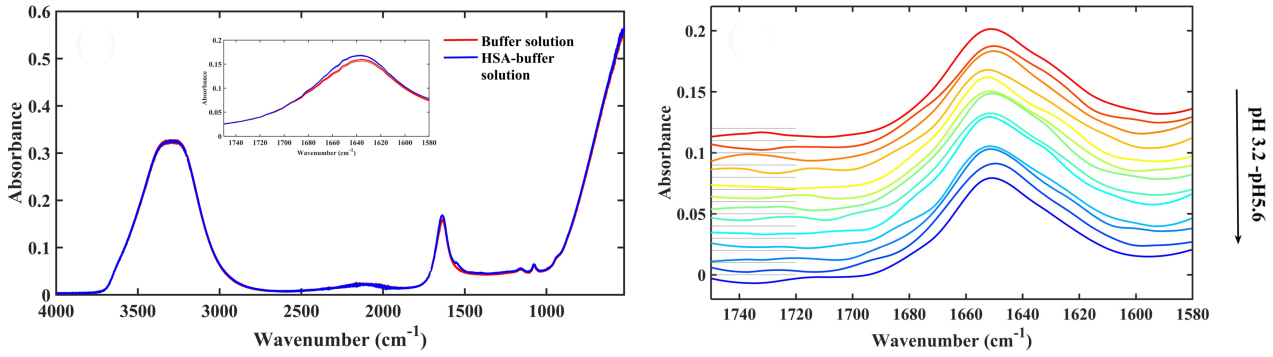


(a) (b)

Fig. 1. (a) IR spectra in the 4000–500 $cm^{-1}$ region of HSA in buffer solution (30 mg/mL) (red) and buffer solution (blue) of pH 5.6–3.2 with a step of pH 0.2. The inset is an enlarged view of the 1750–1580 $cm^{-1}$ region. (b) The IR difference spectra of HSA buffer solution (30 mg/mL). The wavenumber range is 1750–1580 $cm^{-1}$ and the pH is 5.6–3.2 with an interval of 0.2. The difference spectrum was calculated as the IR spectrum of the HSA buffer solution minus the IR spectrum of the buffer solution corresponding to the pH.

the C=O stretching vibration of the peptide group, it is the result of the overlap of C=O bond absorption in different secondary structures and contains information about the secondary structure of the protein such as $\alpha$-helix, $\beta$-sheet, $\beta$-turn, and random coil.[31]

### 3.1.2. *The MW-2DCOS analysis in the 1750–1580 $cm^{-1}$ region*

To visualize the changing characteristics of the spectral intensity during the perturbation process and determine the location of the characteristic peaks, the MW-2DCOS[32,33] was applied on the difference spectra in the region 1750–1580 $cm^{-1}$ and displayed in Fig. 2. It could be found that as the pH decreased, the most prominent variations of the absorption peaks were found at 1656 $cm^{-1}$ and 1633 $cm^{-1}$, which belonged to the $\alpha$-helix and intermolecular $\beta$-sheet structure of HSA, respectively.[30] In addition, relatively weak intensity changes appeared at 1750–1690 $cm^{-1}$, 1602 $cm^{-1}$, and 1598 $cm^{-1}$. According to the previous study,[34] the absorption peaks at 1750–1690 $cm^{-1}$ may be regarded as the absorption resulting from stretching vibration of carboxyl groups with different hydrogen bonding strengths of the acidic residues glutamic acid (Glu) and aspartic acid (Asp) in the HSA side chain. The absorption peak at 1600 $cm^{-1}$ could be assigned to the COO-antisymmetric stretching vibration mode of Glu and Asp residues in HSA.[33] It could be seen from Fig. 2 that when the pH dropped to around 4.6, the energy absorption of the

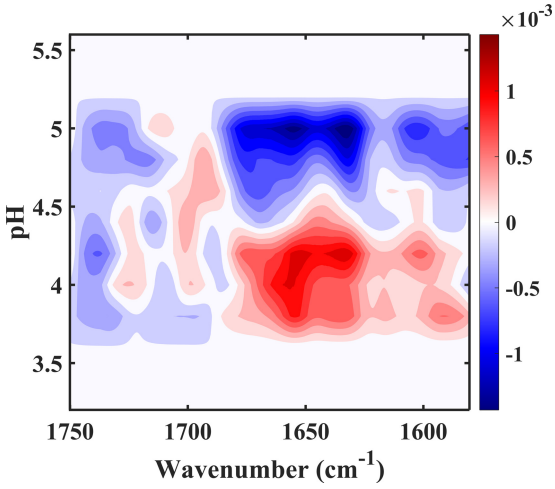


Fig. 2. Moving window two-dimensional plots with autocorrelations calculated from the difference IR spectra in the 1750–1580 $cm^{-1}$ region of HSA in buffer solutions (30 mg/mL). The window size is 5 and the contour level is 8. Red shading indicates that the peak increases with increasing ethanol concentration, while blue shading indicates that the peak intensity decreases with increasing ethanol concentration. As shown on the scale (relative units), the darker the red or blue shading, the tighter the profile, and the greater the change in intensity.

synchronous spectrum at 1690–1580 $cm^{-1}$ changed from negative to positive, which meant that around pH 4.6, the secondary structure of HSA was having relatively significant changes. This is consistent with the previous studies which reported that HSA transitions from N to F was confirmed at a pH of around 4.5.[35–37]

To further explore the pH-induced changes in the secondary structure and side chain groups of HSA, a

segmental analysis was performed according to the results in Fig. 2. Three conformational states of HSA were analyzed by generalized two-dimensional correlation spectroscopy, namely N conformation (normal formation, pH 5.6–4.4), N-F conformation (normal formation-fast migrating formation, pH 4.6–3.8), and F conformation (fast migrating formation, pH 4.0–3.2).[2]

### 3.1.3. *Study on the N conformation of HSA*

The two-dimensional correlated synchronous (a) and asynchronous (b) spectra of HSA buffer solutions at pH 5.6–4.4 within the scope of 1750–1580 $cm^{-1}$ are shown in Fig. 3. A broad autocorrelation peak was formed at 1639 $cm^{-1}$ in the synchronous spectrum, which may include other secondary structure changes due to the broadness of this peak. One negative cross peak (1694 $cm^{-1}$, 1656 $cm^{-1}$) and two positive cross peaks (1718 $cm^{-1}$, 1620 $cm^{-1}$), (1656 $cm^{-1}$, 1620 $cm^{-1}$) in the asynchronous spectrum could be resolved. To determine the sequence order of each secondary structure transition of HSA under different pH induction, it was judged according to Noda's law,[38] as shown in Table 1. From the positive and negative values of the different cross peaks in Table 1, it could be seen that the sequence of changes in the peak intensity of the subpeaks of HSA in N conformation induced by different pH was 1718 $cm^{-1}$ > 1656 $cm^{-1}$ > 1694/1620 $cm^{-1}$, that is, the corresponding weakly hydrogen-bonded COOH group (1718 $cm^{-1}$) was the first to change under acidic pH induction, followed by the $\alpha$-helix structure (absorption peak at low wavenumber 1656 $cm^{-1}$), and lastly the $\beta$-sheet structure (absorption peak at high wave number 1694 $cm^{-1}$ and low wave number 1620 $cm^{-1}$). In consequence, the asynchronous spectrum of the N conformation of HSA suggested that the change in secondary structure was later than the change of the side chain group and the protonation of the COO– group, and the carboxyl group protonation may be the trigger of the secondary structure change.

### 3.1.4. *Study on the N-F conformation of HSA*

The two-dimensional correlated synchronous (c) and asynchronous (d) spectra of HSA buffer difference IR spectra within the scope of 1750–1580 $cm^{-1}$ for pH 4.6–3.8 are shown in Fig. 3. The synchronous spectrum formed a broad autocorrelation peak near 1639 $cm^{-1}$ and a negative crossover peak at 1706 $cm^{-1}$ and 1641 $cm^{-1}$. The absorption peak at 1706 $cm^{-1}$ could be referred to as the absorption of hydrogen-bonded COOH group of moderate intensity, while the absorption peak at 1641 $cm^{-1}$ was considered to be related to the absorption of $\alpha$-helix structure,[30,34] both forming synchronous negative crossover peaks, which indicated that the hydrogen-bonded COOH group and the $\alpha$-helix structure changed in opposite directions of intensity during the N-F conformational change. Three positive cross peaks (1670 $cm^{-1}$, 1641 $cm^{-1}$), (1745 $cm^{-1}$, 1700–1600 $cm^{-1}$), (1700 $cm^{-1}$, 1700–1600 $cm^{-1}$) and one negative cross peak (1641 $cm^{-1}$, 1618 $cm^{-1}$) in the asynchronous spectrum could be distinguished. The presence of more absorption peaks in the N-F conformational change compared to the asynchronous spectrum of the N conformation suggested that several secondary structures of HSA were involved in the change at this stage. One of the absorption peaks at 1745 $cm^{-1}$ was related to the absorption of the free COOH group, which may arise from the unfolding of the HSA structural domain III.[34]

To determine the sequence order of each secondary structure transition of HSA under different pH induction, it was judged according to Noda's rule.[38] From Table 2, it could be observed that the sequence order of pH-induced peak intensity changes of subpeaks of HSA in N-F conformation was 1745/1700 $cm^{-1}$ > 1618 $cm^{-1}$ > 1670 $cm^{-1}$ > 1630 $cm^{-1}$ > 1641 $cm^{-1}$. Therefore, asynchronous spectroscopy studies suggested that carboxyl protonation occurred first in the N-F conformational change of proteins, which then triggered the formation of intermolecular $\beta$-sheet structures, which may be an important process in the intermolecular aggregation of proteins. The change in the intermolecular $\beta$-sheet structure further induced a sequential change in the $\beta$-turn, $\beta$-strand, and $\alpha$-helix structures. This order of change was similar to that of HSA in *N* conformation, but the order of change of $\beta$-sheet and $\beta$-turn structure and $\alpha$-helix structure was different, probably because HSA was more inclined to undergo intermolecular aggregation in a relatively low isoelectric point pH environment.

### 3.1.5. *Study on the F conformation of HSA*

The two-dimensional correlated synchronous (e) and asynchronous (f) spectra of HSA buffer IR

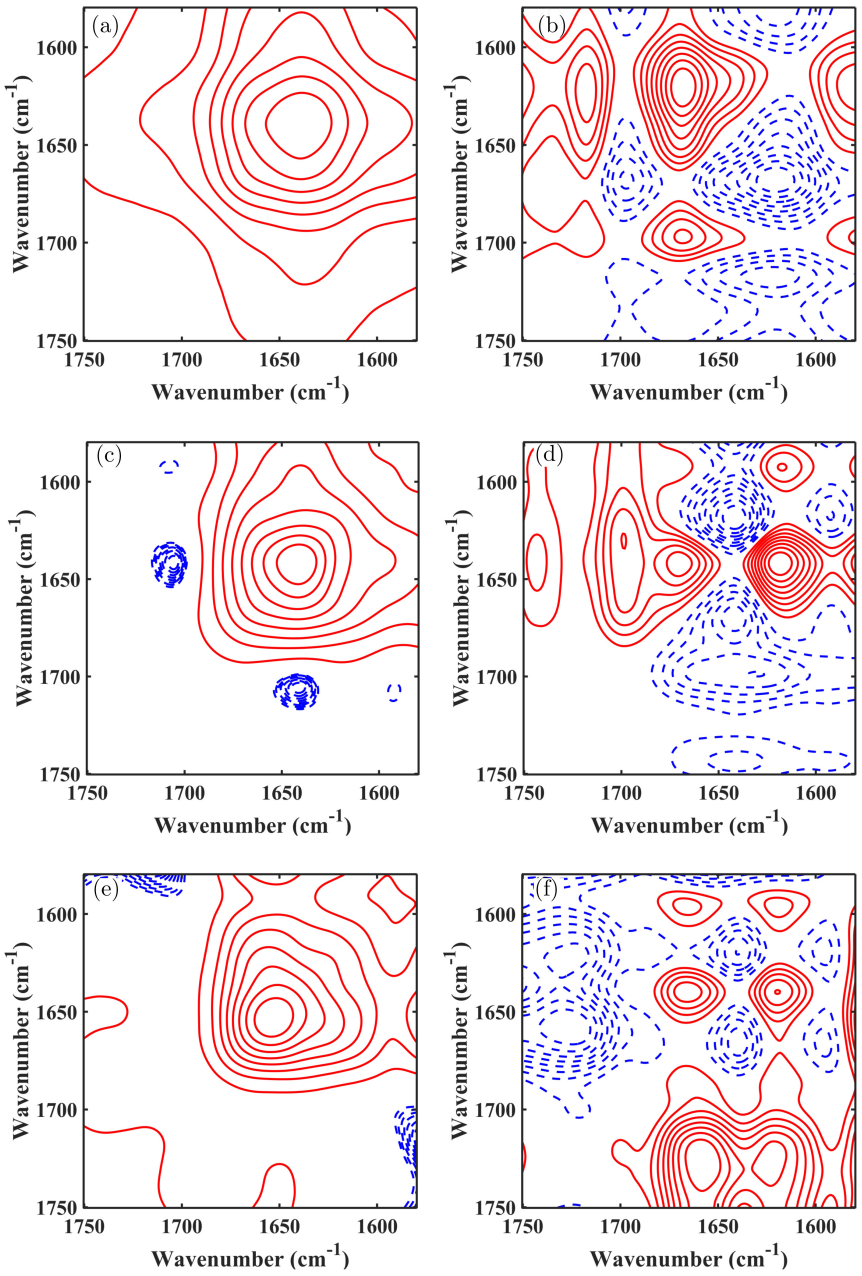


Fig. 3. Synchronous (a) and asynchronous (b), Synchronous (c) and asynchronous (d) and Synchronous (e) and asynchronous (f) two-dimensional IR correlation spectrum in the 1750–1580 $cm^{-1}$ region constructed from pH-dependent (pH 5.6–4.4), (pH 4.6–3.8), and (pH 4.0–3.2) spectral variation of the HSA solutions, respectively. The contour level is 8. The blue dotted lines indicate a negative sign and the red solid lines indicate a positive sign.

spectra within the scope of 1750–1580 $cm^{-1}$ at pH 4.0–3.2 are shown in Fig. 3. The formation of a significant synchronous autocorrelation peak at 1656 $cm^{-1}$ could be observed in Fig. 3, which indicated that the change in the $\alpha$-helical structure was dominant during the F conformational change. In the asynchronous spectrum, more absorption peaks were distinguished, including positive cross peaks (1656 $cm^{-1}$, 1596 $cm^{-1}$), (1656 $cm^{-1}$, 1639 $cm^{-1}$), (1618 $cm^{-1}$, 1596 $cm^{-1}$) and negative cross peaks (1725 $cm^{-1}$, 1656 $cm^{-1}$), (1725 $cm^{-1}$, 1618 $cm^{-1}$). Among them, the absorption peak at 1639 $cm^{-1}$ was caused by the $\beta$-strand structure, while the absorption peak at 1725 $cm^{-1}$ could be attributed to the COOH group bound by moderately strong hydrogen bonds.[30]

Table 1. The signs of the cross peaks in synchronous and asynchronous correlation spectra and "sequential order" analysis of HSA induced by different pH (pH 5.6–4.4).

| ($v_1$, $v_2$, $cm^{-1}$) | $\varphi$ (synchronous) | $\psi$ (asynchronous) | Order ($cm^{-1}$) |
|---|---|---|---|
| (1718, 1620) | + | + | 1718 > 1620 |
| (1656, 1620) | + | + | 1656 > 1620 |
| (1694, 1656) | + | − | 1656 > 1694 |

Table 2. The signs of the cross peaks in synchronous and asynchronous correlation spectra and "sequential order" analysis of HSA induced by different pH (pH 4.6–3.8).

| ($v_1$, $v_2$, $cm^{-1}$) | $\varphi$ (synchronous) | $\psi$ (asynchronous) | Order ($cm^{-1}$) |
|---|---|---|---|
| (1700, 1630) | + | + | 1700 > 1630 |
| (1745, 1641) | + | + | 1745 > 1641 |
| (1670, 1641) | + | + | 1670 > 1641 |
| (1641, 1618) | + | − | 1618 > 1641 |

Table 3. The signs of the cross peaks in synchronous and asynchronous correlation spectra and "sequential order" analysis of HSA induced by different pH (pH 4.0–3.2).

| ($v_1$, $v_2$, $cm^{-1}$) | $\varphi$ (synchronous) | $\psi$ (asynchronous) | Order ($cm^{-1}$) |
|---|---|---|---|
| (1725, 1656) | + | − | 1656 > 1725 |
| (1725, 1618) | + | − | 1618 > 1725 |
| (1656, 1639) | + | + | 1656 > 1639 |
| (1639, 1618) | + | − | 1618 > 1639 |

To determine the sequence order of each secondary structure transition of HSA under different pH induction, a determination was made according to Noda's law.[38] From Table 3, it could be judged that the sequence of pH-induced changes in subpeak peak intensities of HSA in the F conformation was $1618\,cm^{-1} > 1656\,cm^{-1} > 1639\,cm^{-1} > 1725\,cm^{-1}$. Therefore, the increase of intermolecular $\beta$-sheet structure in the $F$ conformation further caused the unfolding of HSA, followed by changes in the $\beta$-strand structure and the side chain carboxyl group.

### 3.2. *Study of the effect of ethanol on structural changes of at the isoelectric point*

The above study showed that different pH affect the secondary structure of albumin and that a significant change starts to occur around pH=4.5, which is also its isoelectric point. Therefore, in this part of the study, ethanol precipitation was performed at the isoelectric point with reference to the characteristics of the production process to observe the pattern of its secondary structure and hydration.

To demonstrate the effect of ethanol on the structure of HSA, the original IR spectra of ethanol-water buffer solution and ethanol–HSA buffer solution are shown in Fig. 4(a). Three distinct absorption peaks around $3300\,cm^{-1}$, $1640\,cm^{-1}$, and $1100\,cm^{-1}$ could be observed in Fig. 4(a). The obvious and broad absorption peak from $3500\,cm^{-1}$ to $3000\,cm^{-1}$ was due to the stretching vibrational absorption of O–H and N–H groups since water, ethanol, and proteins are all rich in O–H groups.[28] In addition, the absorption peak that appeared at $1640\,cm^{-1}$ was mainly associated with the flexural vibration of the O–H group of HSA and the stretching vibration of the C=O group.[28] Furthermore, it could also be seen from the enlarged image of the $1750–1580\,cm^{-1}$ region that with the increase of ethanol concentration, the absorption peak shifted to higher numbers, which indicated a change in the hydrogen bonding network.

To eliminate the interference caused by strong background absorption and obtain more information about HSA, a difference spectrum was obtained by the spectra of ethanol–HSA buffer solution and the corresponding ethanol–water buffer solution. Previous studies had shown that the absorption bands of proteins in IR spectra included many characteristic absorption bands, among which the amide I region was associated with the C=O stretching vibrations.[31] Therefore, the difference spectra of HSA buffer (30 mg/mL) with different ethanol concentration at $1750–1580\,cm^{-1}$ is shown in Fig. 4(b), where the absorption peak near $1652\,cm^{-1}$ was attributed to the vibrational absorption in the amide I region. It could also be noted that the peak intensities caused by different ethanol concentrations are inconsistent, indicating that ethanol affects the amide I region differently.

As an effective way to directly observe the spectral intensity change under the disturbance, MW-2DCOS[39] was adopted to gain more insights into the protein structure correlation under the perturbation of ethanol. The MW-2DCOS plots with auto-correlations and its power spectrum calculated from the difference spectrum within the scope of $1750–1580\,cm^{-1}$ for different ethanol concentrations of HSA buffer solution (30 mg/mL) are

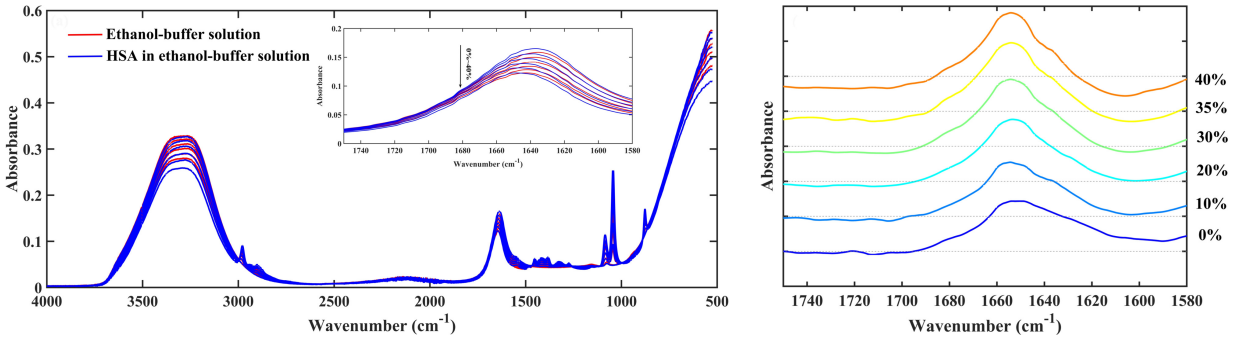


Fig. 4. (a) IR spectra in the 4000–500 $cm^{-1}$ region of ethanol–water buffer solution (red) and HSA buffer solution (30 mg/mL) with different ethanol concentrations (blue). The inset is an enlarged view of the 1750–1580 $cm^{-1}$ region. (b) The difference spectra in the 1750–1580 $cm^{-1}$ region of HSA buffer solution (30 mg/mL) with different ethanol concentrations.

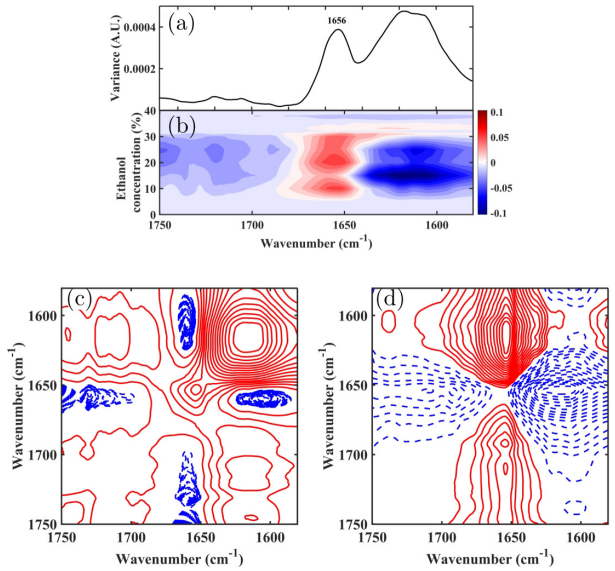


Fig. 5. Moving window two-dimensional plots with auto-correlations (a) and its power spectrum (b) calculated from the difference spectra in the 1750–1580 $cm^{-1}$ region of HSA buffer solutions (30 mg/mL) with different ethanol concentrations. The window size is 5 and the contour level is 16. Red shading indicates that the peak increases with increasing ethanol concentration, while blue shading indicates that the peak intensity decreases with increasing ethanol concentration. As shown on the scale (relative units), the darker the red or blue shading, the tighter the profile, and the greater the change in intensity. Synchronous (c) and asynchronous (d) 2D IR correlation spectrum in the 1750–1580 $cm^{-1}$ region constructed from the difference IR spectra of HSA solutions (30 mg/mL) with different ethanol concentrations. The contour level is 16. The blue dotted lines indicate a negative sign and the red solid lines indicate a positive sign.

displayed in Fig. 5. The most pronounced variation in the intensity of the absorption peaks at 1656 $cm^{-1}$ and 1621 $cm^{-1}$ could be observed in the figure, which was attributed to the $\alpha$-helix and intermolecular $\beta$-sheet structure of HSA, respectively.[30] Furthermore, the weak absorption peaks formed in the range of 1750–1690 $cm^{-1}$ were mainly associated with the absorption of the side chain carboxyl groups. The peak intensity rate of change of 1656 $cm^{-1}$ and 1621 $cm^{-1}$ absorption peaks reached the maximum at an ethanol concentration of 20% indicating a maximum second structure change rate. It could be seen from the peak intensities that the main change in this process was the formation of the intermolecular $\beta$-sheet structure. The intensity of the absorption peak corresponding to the $\alpha$-helix structure kept a positive value when the ethanol concentration was lower than 30%, indicating the enhancement of $\alpha$-helix structure stability with ethanol. When the ethanol concentration was lower than 40%, the absorption peak intensity corresponding to the $\beta$-sheet structure became negative, which means that the intermolecular $\beta$-sheet structure increased and was exposed to the solvent. As the ethanol concentration was higher than 30%, the absorption peak at 1656 $cm^{-1}$ changed from a positive value to a negative value, while the absorption peak value at 1621 $cm^{-1}$ changed from negative to positive, and these may be correlated with the protein precipitation phenomenon observed in the experiment. It could be deduced that the excessive addition of ethanol may cause the destruction of the structure of HSA, exposing the $\alpha$-helix structure to the solvent. The formation of intermolecular $\beta$-sheet structure was also considered to be an essential reason for protein aggregation and precipitation.

To eliminate the effect of noise, 2DCOS analysis was performed on the difference IR spectra of HSA solution (30 mg/ml) in the region of 1750–1580 $cm^{-1}$.

Table 4. The signs of the cross peaks and "sequential order" analysis of HSA induced by different ethanol concentrations.

| ($v_1$, $v_2$, $cm^{-1}$) | $\varphi$ (synchronous) | $\psi$ (asynchronous) | Order ($cm^{-1}$) |
|---|---|---|---|
| (1656, 1621) | − | + | 1621 > 1656 |
| (1729, 1656) | − | − | 1729 > 1656 |
| (1729, 1621) | + | + | 1729 > 1621 |

The synchronous (c) and asynchronous (d) of 2DCOS are displayed in Fig. 5. There were two autocorrelation peaks in the simultaneous spectra of Fig. 5(c), 1656 $cm^{-1}$ and 1621 $cm^{-1}$, respectively, where the latter was significantly stronger in intensity than the former, indicating that the main change in the system was the formation of intermolecular $\beta$-sheet. The two negative cross-peaks formed at (1656 $cm^{-1}$, 1621 $cm^{-1}$) and (1656 $cm^{-1}$, 1729 $cm^{-1}$) indicated that the changing direction of $\alpha$-helix and $\beta$-sheet and side chain structures were opposite. A positive cross-peak was formed at (1729 $cm^{-1}$ and 1621 $cm^{-1}$), indicating that the two corresponding structures had changed in the same direction, and there was a strong synergy between them. The peak at 1729 $cm^{-1}$ could be assigned to the absorption of weakly hydrogen-bonded carboxyl groups.[30]

In the asynchronous spectra of Fig. 5(d), 1656 $cm^{-1}$ formed a negative cross-peak with 1750–1654 $cm^{-1}$, and a positive cross-peak with 1656–1580 $cm^{-1}$, indicating that 1656 $cm^{-1}$ was closely related to other secondary structures and side chain groups were heterogeneously cross-correlated. According to Noda law,[38] the sequential order was 1729 $cm^{-1}$ > 1621 $cm^{-1}$ > 1656 $cm^{-1}$ as seen in Table 4. The COOH groups with varying degrees of hydrogen bonds continuously changed with increasing ethanol concentration, which in turn caused changes in the intermolecular $\beta$-sheet structure, promoted protein precipitation, and finally caused the enhancement of the $\alpha$-helix structure. This may be due to the accelerated dehydration of HSA under the synergistic effect of isoelectric pH and ethanol, which first promoted the formation of intermolecular $\beta$-sheet structure and then triggered the precipitation.

### 3.3. *NIR spectra of ethanol–water and ethanol–water with HSA solutions*

The NIR spectra of different concentrations of ethanol–buffer solution and HSA buffer solution of diverse ethanol concentrations are displayed in Fig. 6, where two main distinct absorption peaks around 6900 $cm^{-1}$ and 5100 $cm^{-1}$ could be observed. The broad peak near 6900 $cm^{-1}$ could be attributed to the combined frequency absorption of the symmetric and antisymmetric stretching vibrations of the O–H bond ($v_1 + v_3$), and the strong absorption peak near 5100 $cm^{-1}$ was related to the combined frequency of the bending vibration and the antisymmetric stretching vibration of the O–H group ($v_2 + v_3$).[40,41] It could be observed that the absorbance intensity reduced with the increase of ethanol and shifted toward a higher wavenumber in the 7300–6200 $cm^{-1}$ region, which was mainly associated with the reduction of water and changes in the

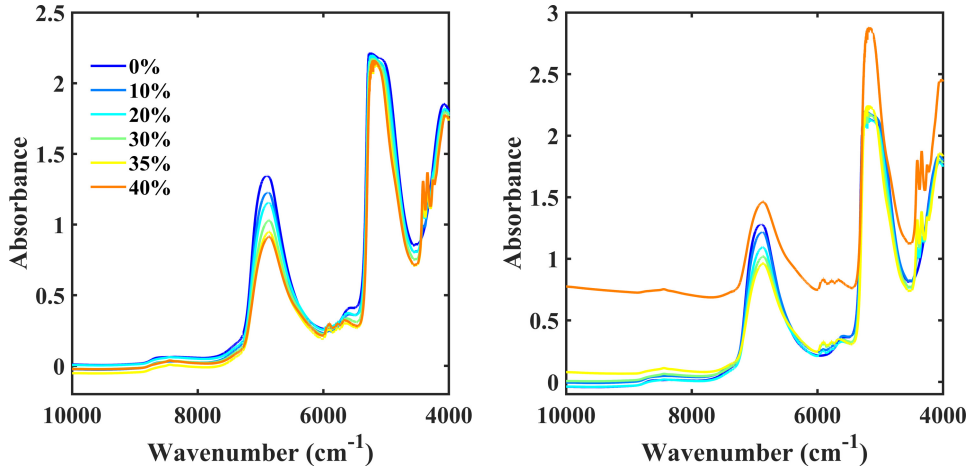


(a) (b)

Fig. 6. (a) NIR spectra of ethanol–buffer solution (b) and HSA in buffer solutions with different ethanol concentrations.

hydrogen bond network. Furthermore, it can be observed in Fig. 6 (b) that at ethanol concentrations of 35% and 40%, the HSA produced significant turbidity and precipitation, which caused significant light scattering and eventually led to a significant baseline drift in the NIR spectra.

### 3.3.1. *Analysis of hydration water with difference spectrum*

The difference spectrum was used to reduce the strong interference caused by solvent absorption, and the variations in HSA hydration induced by ethanol could be further investigated. After baseline correction in the spectra range of 7940–6015 $cm^{-1}$, the difference spectra of HSA buffer solutions with different ethanol concentrations and the corresponding ethanol–buffer solutions were performed and reproduced in Fig. 7(a). It could be seen from the figure that the difference spectrum peak gradually decreased with increasing ethanol concentration and changed from a negative value to a positive value at 40% concentration due to a large amount of protein precipitation. Since the data was no longer accurate, only the difference spectrum of HSA buffer in the range of 0–35% ethanol concentration was discussed below.

By analyzing the difference spectra of Fig. 7(a), we deduced that the information affecting the difference spectra mainly came from three factors, namely (a) exclusion volume effect, (b) hydration effect, and (c) the absorption of HSA. First, under the same illumination condition, the NIR absorption of HSA buffer solution with different ethanol concentrations was always smaller than those of the corresponding concentrations of the ethanol–buffer solution, resulting in the negative contribution of excluded volume effect to the difference spectrum. Second, the addition of ethanol caused changes in the structure of the water molecules surrounding the protein. If the NIR spectrum of hydrated water differed from that of the ethanol–water buffer, then hydration contributed positively to the difference spectrum. Third, unlike water, the absorption of HSA contributes positively to the difference spectrum. Because HSA concentrations were consistent across the studied systems, it could be speculated that the differences in spectral intensities were mainly caused by changes in hydration effects.

To gain a deeper understanding of the hydration effect caused by ethanol, the integrated intensity of the NIR difference spectra in Fig. 7(a) was calculated, and the results are shown in Fig. 7(b), which showed that the integrated intensity decreased rapidly with increasing ethanol concentration, and when the ethanol concentration was 35%, the decreasing speed was accelerated. It should be pointed out that a smaller integral value represents a stronger contribution to the hydration effect and vice versa. Therefore, it could be speculated that the hydrated water on the protein surface decreased almost linearly with increasing ethanol concentration from 0–30% ethanol. Aggregation and precipitation of proteins in 35% ethanol conditions resulted in a small reduction in the amount of hydrated water around the protein, which may be related to the

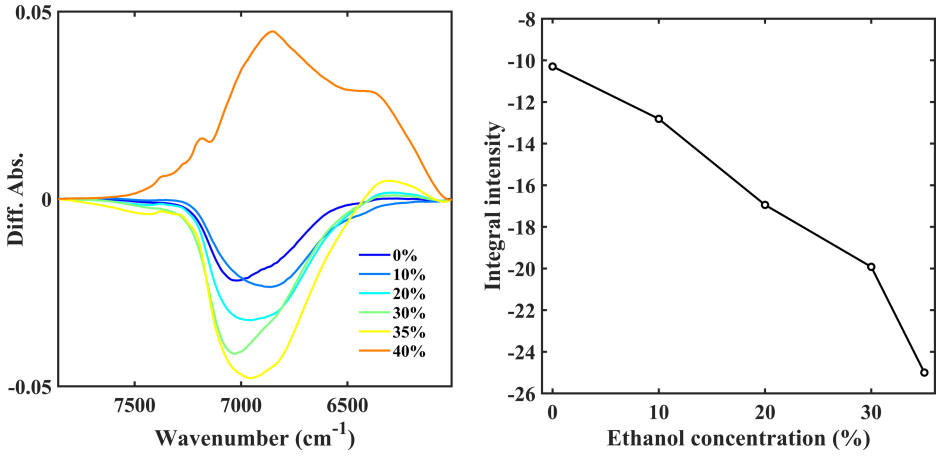


(a) (b)

Fig. 7. (a) The difference between NIR spectra (b) in the 7940–6015 $cm^{-1}$ region of HSA solution (30 mg/mL) with different ethanol concentrations and the integral intensity of NIR difference spectra.

reduction of bound water due to the reduction of the surface area after protein aggregation.

### 3.3.2. *Analysis of hydration water with the McCabe–Fisher method*

To acquire further information on the hydration layer, the above-mentioned difference spectra were analyzed using the McCabe–Fisher method.[42] The resolution of the difference spectra of HSA buffer solution with 30% ethanol concentration is shown in Fig. 8(a), and the hydration spectra calculated are displayed in Fig. 8(b). According to this method, it could be concluded that the difference spectrum (curve A) (Fig. 8(a)) was influenced by the totality of the three factors: (a) The negative contribution of the excluded volume effect to the difference spectrum is because more water molecules are absorbed in the reference cell than in the sample cell. (b) If the NIR spectrum of hydrated water is different from the spectrum of water in the ethanol–water buffer solution in the reference cell, then the contribution of hydration to curve A is positive. (c) Since the absorption of HSA in the studied NIR spectral region is different from that of water, the contribution to curve A may be positive. It is important to note that HSA concentrations were consistent across the systems studied, the contribution of factor (a) and factor (c) was consistent, and factor (b) was the main cause of the difference spectrum. To obtain more information about the structural changes of ethanol and water in the hydrated layer, the difference spectrum was decomposed into two component spectra (curves B and C), where curve B (factor a) represents the net contribution of the reference solvent and curve C (factors b and c) is derived from the absorption spectra produced by HSA and hydrating water. The absorbance values of the pure solvent spectra over all wavenumbers are multiplied by the normalization factor to obtain Curve B.[43] Since only the solvent is present in the cuvette, the shape of curve B must be the same as the spectrum of the ethanol–water solution. Curve C (absorption spectra of HSA and hydrated water) is obtained by summing the curves A and B of different wavenumbers. Curve A was resolved using the McCabe–Fisher method for all ethanol concentrations, and the results of the resolution of the difference spectra of HSA solutions at 30% ethanol concentration are shown in Fig. 8(b). The results showed that the absorbance of the hydration spectrum gradually decreased with increasing ethanol concentration. Since HSA undergoes significant turbidity and precipitation at 35% and 40% ethanol concentrations, resulting in an inhomogeneous system and spectral drift, this method is not applicable and will not be discussed.

### 3.3.3. *Analysis of hydration water with acquaphotomics*

Aquaphotomics was used to further investigate the structural changes in water associated with ethanol-induced protein precipitation. An aquagram was

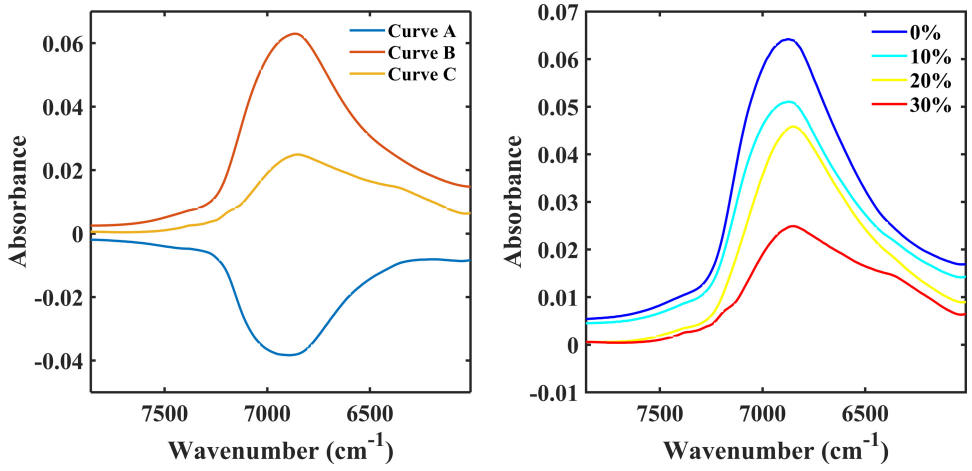


Fig. 8. The resolution of the difference spectrum of HSA solution with 30% ethanol concentration using the (a) McCabe–Fisher method and (b) the calculated hydration spectra.

Table 5. Water matrix co-ordinates (WAMACS): The characteristic water absorbance bands in NIR spectral band.[44–47]

| Wavenumber ($cm^{-1}$) | Water characteristic attributes |
|---|---|
| 7440 | $2v_3$: $H_2O$ asymmetric stretching vibration |
| 7349 | $OH–(H_2O)_{1,2,4}$: Water solvation shell |
| 7270 | $v_1 + v_3$: Symmetrical stretching vibration and $H_2O$ asymmetric stretching vibration |
| 7234 | $OH–(H_2O)_{1,4}$: Water solvation shell; $O_2–(H_2O)_4$: Hydrated superoxide clusters; $2v_1$: $H_2O$ symmetrical stretching vibration; |
| 7072 | water confined in a local field of ions; $S_0$: Free water, water with free $OH^-$ |
| 7037 | free water, water with free, H–OH bond, and O–H...O |
| 6941 | $S_1$: Water molecules with one hydrogen bond |
| 6906 | $OH–(H_2O)_{4,5}$: Water solvation shell |
| 6821 | $S_2$: Water molecules with two hydrogen bonds; $2v_2 + v_3$: $H_2O$ bending and asymmetrical stretching vibration |
| 6784 | $S_3$: Water molecules with three hydrogen bonds |
| 6705 | $S_4$: Water molecules with four hydrogen bonds |
| 6607 | $v_1$: $H_2O$ symmetrical stretching vibration; $v_2$: $H_2O$ bending vibration; strongly bound water |

*Notes*: $^{an}S_n$ represents water molecules with $n$ hydrogen bonds, such as $S_1$ means water molecules with one hydrogen bond.

constructed using the 12 characteristic water wave numbers (Table 5) of the water matrix coordinates (WAMACS) defined by Tsenkova *et al.*,[44–46] which can visualize the spectral patterns of water at different ethanol concentrations. The values of the aquagram were derived from the following equation:

$$A_\lambda^{'} = (A_\lambda - \mu_\lambda)/\sigma_\lambda, \quad (1)$$

where $A_\lambda$ is the absorbance after multiplicative scatter correction (MSC), $\mu_\lambda$ and $\sigma_\lambda$ are the averages of all spectra at wavelength $\lambda$ (converted to wavenumber in this paper) and the standard deviation of all spectra, respectively.

The aquagram pattern of the effect of ethanol concentration on the HSA hydration spectrum is shown in Fig. 9. It can be observed from the figure

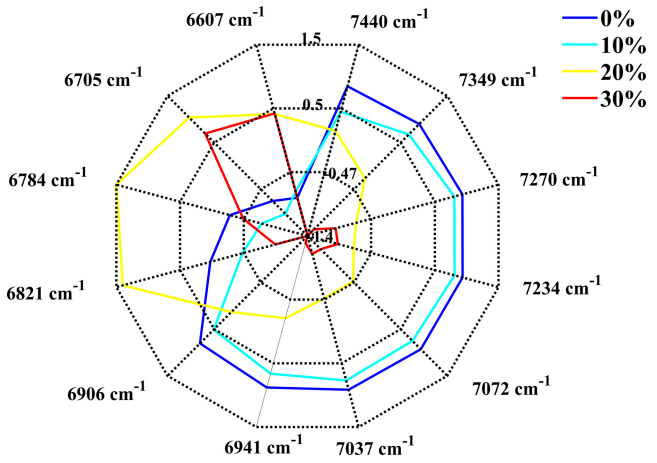


Fig. 9. Ethanol concentration dependency of water spectral changes depicted by aquagram patterns.

that the hydration spectrum first shifted toward lower wave numbers as the ethanol concentration increased, indicating a shift from a water structure with less hydrogen bonded to a water cluster with more hydrogen bonded. At 20% ethanol concentration, the wavenumbers of 6821 $cm^{-1}$ ($S_2$), 6784 $cm^{-1}$ ($S_3$), and 6705 $cm^{-1}$ ($S_4$) changed significantly, which implied an enhancement of the hydrogen-bonded water cluster from 0% to 20% concentration. However, as the ethanol concentration continued to increase from 20% to 30%, the absorbance of water began to shift to a higher wavenumber (shorter wavelength), indicating that hydrated water tends to form a relatively weak hydrogen-bonded water cluster. Therefore, it is not difficult to find that the change process of the hydration structure under the influence of ethanol is nonlinear, that is, free water molecules or weakly hydrogen-bonded water molecules are dominated at low ethanol concentrations ($\leq$20%), and the hydration layer develops into a strongly hydrogen-bonded water cluster with increasing ethanol concentration. These water clusters play essential roles in connecting individual protein molecules, which may be necessary for protein nucleation and precipitation.[48] With the aggregation of the protein, the hydrogen bond network of water gradually became weaker and released into the native water as free water, and the hydration effect was weakened, which was consistent with the results of the volume effect study. When the ethanol concentration rose above 30%, HSA precipitated clearly. Meanwhile, the wavenumbers at 7072 $cm^{-1}$ ($S_0$), 7234 $cm^{-1}$,

and 7270 $cm^{-1}$ in Fig. 9 shifted significantly to high wavenumbers, which is consistent with the insulin amyloid fibrillation study.[48] During the extended phase of protein precipitation, protein molecules approached each other and the surface area gradually decreased. The disintegration of the hydrogen-bonded water cluster then led to an increase in free water and enhanced the bending and stretching vibrations of water. Thus, hydration plays an important role in the alcoholic precipitation of HSA.

## 4. Conclusion

In this work, we first investigated the effect of acidic pH (pH 5.6–3.2) on the secondary structure of HSA using IR spectroscopy. A significant change in the secondary structure of HSA near pH 4.6, a shift from the N conformation to the F conformation, was identified by MW-2DCOS analysis. Then, the MW-2DCOS analysis was used to segment the N conformation, N-F conformation, and F conformation of HSA. It was found that the carboxyl group protonated the side chain Asp and Glu residues of HSA might be important in inducing the secondary structure change. Secondly, we explored the mechanism of precipitation induced by the addition of ethanol using IR and NIR spectra. The synchronous and asynchronous results demonstrated that the native structure of HSA could be achieved by enhancing the $\alpha$-helix structure with low concentrations of ethanol. Meanwhile, at the isoelectric point pH, ethanol has the effect of promoting the formation of intermolecular $\beta$-sheet structure, which is an essential reason for the aggregated precipitation of HSA. The integrated intensities and hydration spectra were obtained according to the McCabe–Fisher method. The variation of the integral intensity proved that ethanol at the isoelectric point pH affected the amount of hydrated water around the protein. The water spectroscopy histology theory was also applied to analyze the hydration layer water structure, which confirmed that water molecules with different degrees of hydrogen bond were involved in different precipitation stages of HSA. In addition, the isoelectric point pH and ethanol were shown to have a synergistic effect on the hydration process of HSA by IR and NIR spectroscopic studies. The research in this paper provided an important theoretical basis for the selection of process parameters for the ethanol precipitation of plasma proteins and the purification of HSA and provided key scientific support for optimizing the existing production process and obtaining high-quality plasma protein products.

## Acknowledgments

We are grateful for the financial support of the National Key Research and Development Program of China (Grant Numbers 2021YFB3201200 and 2021YFB3201202) and the Shandong Province Natural Science Foundation (Grant Numbers ZR2021QB177 and ZR2022QB205). H. Zhang and M. Liang contributed equally to this work and should be regarded as co-first authors.

## Conflict of Interest

The authors declare no conflicts of interest.

## References

1. A. M. Pollock, *Structural and Functional Modification of Human Serum Albumin by Lipid Peroxidation By-Products* (Duquesne University ProQuest Dissertations Publishing, USA, 2005).
2. D. C. Carter, J. X. Ho, "Structure of serum-albumin," *Adv. Protein Chem.* **45**, 153–203 (1994).
3. T. J. Peters, "All about albumin," *All About Albumin* 319–413 (1995).
4. J. R. Brown, "Structure of serum-albumin," *Abs. Papers Am. Chem. Soc.* **172**(Sep3), 12 (1976).
5. E. J. Cohn, J. L. Oncley, L. E. Strong *et al.*, "Chemical, clinical, and immunological studies on the products of human plasma fractionation. I. The characterization of the protein fractions of human plasma," *J. Clin. Invest.* **23**(4), 417–432 (1944).
6. C. Yang *et al.*, "Investigation of protective effect of ethanol on the natural structure of protein with infrared spectroscopy," *Spectrochim. Acta A-Mol. Biomol. Spectrosc.* **271**, 120935 (2022).
7. K. B. Bec, J. Grabska, C. W. Huck, "Biomolecular and bioanalytical applications of infrared spectroscopy — A review," *Anal. Chim. Acta.* **1133**, 150–177 (2020).
8. S. Pieters *et al.*, "Near-infrared spectroscopy for in-line monitoring of protein unfolding and its interactions with lyoprotectants during freeze-drying," *Anal. Chem.* **84**(2), 947–955 (2012).
9. S. Navea, A. de Juan, R. Tauler, "Modeling temperature-dependent protein structural transitions by combined near-IR and mid-IR spectroscopies and multivariate curve resolution," *Anal. Chem.* **75**(20), 5592–5601 (2003).

10. V. Moll *et al.*, "Investigation of water interaction with polymer matrices by near-infrared (NIR) spectroscopy," *Molecules* **27**(18), 5882 (2022).
11. C. Yu *et al.*, "Determination of the immunoglobulin G precipitation end-point by an intelligent near-infrared spectroscopy system," *J. Innov. Opt. Health Sci.* **14**(3), 2150007 (2021).
12. M. Fan, W. Cai, X. Shao, "Investigating the structural change in protein aqueous solution using temperature-dependent near-infrared spectroscopy and continuous wavelet transform," *Appl. Spectrosc.* **71**(3), 472–479 (2017).
13. L. Ma *et al.*, "Understanding the function of water during the gelation of globular proteins by temperature-dependent near infrared spectroscopy," *Phys. Chem. Chem. Phys.* **20**(30), 20132–20140 (2018).
14. A. Bax, *Two-Dimensional Nuclear Magnetic Resonance in Liquids*, Delft University Press, USA and Canada (1982).
15. S. L. Ma *et al.*, "Two-dimensional vibrational circular dichroism correlation spectroscopy: pH-induced spectral changes in L-alanine," *J. Mol. Struct.* **799**(1–3), 226–238 (2006).
16. R. Tsenkova, Visible-near infrared perturbation spectroscopy: Water in action seen as a source of information, *12th Int. Conf. Near-Infrared Spectroscopy*, Auckland (2005), pp. 607–612.
17. D. J. Wang *et al.*, "Application of near-infrared spectroscopy to agriculture and food analysis," *Guang Pu Xue Yu Guang Pu Fen Xi* **24**(4), 447–450 (2004).
18. Y. Xiong *et al.*, "Quantification of potassium concentration with Vis/SWNIR spectroscopy in fresh lettuce," *J. Innov. Opt. Health Sci.* **13**(6), 2050029 (2020).
19. J. Luypaert, D. L. Massart, Y. Vander Heyden, "Near-infrared spectroscopy applications in pharmaceutical analysis," *Talanta* **72**(3), 865–883 (2007).
20. W. Zeng *et al.*, "Multivariety and multimanufacturer drug identification based on near-infrared spectroscopy and recurrent neural network," *J. Innov. Opt. Health Sci.* **15**(4), 2250022 (2022).
21. S. Zhang *et al.*, "Rapid and simultaneous determination of moisture and berberine content in Coptidis Rhizoma and Phellodendri Chinensis Cortex by near-infrared spectroscopy and chemometrics," *J. Innov. Opt. Health Sci.* **13**(2), 2050006 (2020).
22. A. Wong *et al.*, "Assessment of cerebral oxygenation response to hemodialysis using near-infrared spectroscopy (NIRS): Challenges and solutions," *J. Innov. Opt. Health Sci.* **14**(6), 2150016 (2021).
23. J. Y. Sun *et al.*, "Near-infrared spectroscopy as a promising tool in stroke: Current applications and future perspectives," *J. Innov. Opt. Health Sci.* **14**(6), 2130006 (2021).
24. H. Wang *et al.*, "Spectra selection methods: A novel optimization way for treating dynamic spectra and in-line near infrared modelling," *J. Innov. Opt. Health Sci.* **13**(4), 2050015 (2020).
25. L. Li *et al.*, "Multi-manufacturer drug identification based on near infrared spectroscopy and deep transfer learning," *J. Innov. Opt. Health Sci.* **13**(4), 2050016 (2020).
26. J. Muncan *et al.*, "Aquaphotomics approach for monitoring different steps of purification process in water treatment systems," *Talanta* **206**, 120253 (2020).
27. A. Puttipipatkajorn, A. Puttipipatkajorn, "Development of calibration models for rapid determination of moisture content in rubber sheets using portable near-infrared spectrometers," *J. Innov. Opt. Health Sci.* **13**(2), 2050009 (2020).
28. M. Grossutti, J. R. Dutcher, "Correlation between chain architecture and hydration water structure in polysaccharides," *Biomacromolecules* **17**(3), 1198–1204 (2016).
29. Y. Ozaki *et al.*, *Near-Infrared Spectroscopy: Theory, Spectral Analysis, Instrumentation, and Applications*, Springer, Singapore (2021).
30. Y. Q. Wu, K. Murayama, Y. Ozaki, "Two-dimensional infrared spectroscopy and principle component analysis studies of the secondary structure and kinetics of hydrogen-deuterium exchange of human serum albumin," *J. Phys. Chem. B* **105**(26), 6251–6259 (2001).
31. S. Jiang *et al.*, "Infrared spectroscopy of hydrogen-bonding interactions in neutral dimethylamine-methanol complexes," *J. Phys. Chem. A* **123**(46), 10109–10115 (2019).
32. S. Sasic, A. Muszynski, Y. Ozaki, "A new possibility of the generalized two-dimensional correlation spectroscopy. 1. Sample-sample correlation spectroscopy," *J. Phys. Chem. A* **104**(27), 6380–6387 (2000).
33. S. Morita *et al.*, "Perturbation-correlation moving-window two-dimensional correlation spectroscopy," *Appl. Spectrosc.* **60**(4), 398–406 (2006).
34. K. Murayama *et al.*, "Two-dimensional/attenuated total reflection infrared correlation spectroscopy studies on secondary structural changes in human serum albumin in aqueous solutions: pH-dependent structural changes in the secondary structures and in the hydrogen bondings of side chains," *J. Phys. Chem. B* **105**(20), 4763–4769 (2001).
35. T. Peters, ScienceDirect, *All About Albumin: Biochemistry, Genetics, and Medical Applications*, Academic Press, San Diego (1996).
36. D. C. Carter, J. X. Ho, "Structure of serum albumin," *Adv. Protein Chem.* **45**, 153–203 (1994).
37. S. Era *et al.*, "Cd-resolved secondary structure of bovine plasma-albumin in acid-induced isomerization," *Int. J. Peptide Protein Res.* **22**(3), 333–340 (1983).
38. I. Noda, I. Y. Ozaki, *Two-Dimensional Correlation Spectroscopy: Applications in Vibrational and Optical Spectroscopy*, Wiley, Hoboken (2005).

39. L. Zhang, I. Noda, Y. Wu, "Concatenated two-dimensional correlation analysis: A new possibility for generalized two-dimensional correlation spectroscopy and its application to the examination of process reversibility," *Appl. Spectrosc.* **64**(3), 343–350 (2010).
40. J. Workman, Jr. L. Weyer, *Practical Guide to Interpretive Near-Infrared Spectroscopy*, CRC Press, Boca Raton (2008).
41. M. Zhang *et al.*, "Research on the structure of peanut allergen protein ara h1 based on aquaphotomics," *Front. Nutr.* **8**, 696355 (2021).
42. W. C. Mccabe, H. F. Fisher, "Near-infrared spectroscopic method for investigating the hydration of a solute in aqueous solution," *J. Phys. Chem.* **74** (15), 2990–2998 (1970).
43. Q. Dong *et al.*, "Analysis of hydration water around human serum albumin using near-infrared spectroscopy," *Int. J. Biol. Macromol.* **138**, 927–932 (2019).
44. R. Tsenkova, "Aquaphotomics: dynamic spectroscopy of aqueous and biological systems describes peculiarities of water," *J. Near Infrared Spectrosc.* **17**(6), 303–313 (2009).
45. D. Kojić *et al.*, "Water confined in the local field of ions," *Chem. Phys. Chem.* **15**(18), 4077–4086 (2014).
46. A. A. Gowen *et al.*, "Use of near infrared hyperspectral imaging to identify water matrix co-ordinates in mushrooms (Agaricus bisporus) subjected to mechanical vibration," *J. Near Infrared Spectrosc.* **17**(6), 363–371 (2009).
47. Q. Dong *et al.*, "Understanding hyaluronic acid induced variation of water structure by near-infrared spectroscopy," *Sci. Rep.* **10**(1), 1–8 (2020).
48. E. Chatani *et al.*, "Water molecular system dynamics associated with amyloidogenic nucleation as revealed by real time near infrared spectroscopy and aquaphotomics," *PLoS One* **9**(7), e101997 (2014).